# Dynamic Monte Carlo Simulations of the Oxygen Electroreduction Reaction on a Bimetallic Surface

A Senior Scholars Thesis

by

ADAM WAYNE WOOD

Submitted to the Office of Undergraduate Research
Texas A&M University
in partial fulfillment of the requirements for the designation as

UNIVERSITY UNDERGRADUATE RESEARCH SCHOLAR

April 2006

Major: Chemical Engineering

# Dynamic Monte Carlo Simulations of the Oxygen Electroreduction Reaction on a Bimetallic Surface

A Senior Scholars Thesis

by

ADAM WAYNE WOOD

Submitted to the Office of Undergraduate Research
Texas A&M University
in partial fulfillment of the requirements for the designation as

UNIVERSITY UNDERGRADUATE RESEARCH SCHOLAR

Approved by:

Research Advisor: Perla Balbuena
Associate Dean for Undergraduate Research: Robert C. Webb

April 2006

Major: Chemical Engineering

# ABSTRACT

Dynamic Monte Carlo Simulations of the Oxygen Electroreduction Reaction on a Bimetallic Surface (April 2006)

Adam W. Wood
Department of Chemical Engineering
Texas A&M University

Research Advisor: Dr. Perla B. Balbuena
Department of Chemical Engineering

Platinum and platinum alloy surfaces are used as catalysts to promote the reduction of oxygen, one of the reactions used to generate electrical energy in low temperature fuel cells, which are sought as promissory clean power sources. In such devices, the oxygen reduction is the slowest of the two electrode reactions, significantly affecting the performance of the fuel cell. Oxygen reduction is also important for several biological problems, such as oxygen transport in living organisms. In my research, I analyzed the effect of concentrations of a secondary metal on the overall mechanism of oxygen reduction on platinum alloy catalysts. I employed dynamic Monte Carlo, a simulation program that studies the kinetics of reactions, and returns relevant data that can be analyzed.

To better understand how to improve the oxygen current density, I studied two different cases involving a bimetallic surface. For the first case I employed an initial secondary metal M at varying concentrations with a 100% increase in activation energy for the adsorption of oxygen, but a 10% decrease in activation energy for the other four electron transfer reactions, while the second case I kept the above values, but reduced the activation energy for the adsorption of oxygen to a 10% increase on metal M. I

discovered that between 50 to 70% metal concentration enabled the best sites for reduction for the first case, and 50 to 90% metal concentration enabled the best sites for reduction for the second case. This is particularly important, for if it can be discovered that a secondary metal mixed with platinum can yield the results I discovered, then the reduction of oxygen may become commercially feasible, reducing the cost of the catalyst needed, and by increasing the current density yield resulting in greater reduction performance.

# Table of Contents

# List of Figures

# List of Tables

## 1. Introduction

The oxygen reduction reaction (ORR) attracts considerable interest because of its essential role in low-temperature fuel cells. The overall reaction in an acidic medium is,

$$O_2 + 4e^- + 4H^+ \rightarrow 2H_2O$$

It is generally accepted that the cathodic ORR is more difficult to be catalyzed than the anodic oxidation reaction of a fuel like $H_2$, and that considerable overpotential and consequent energy loss arise from its slow kinetics even catalyzed by Pt, the most active cathode catalyst. Despite a great deal of effort oriented to elucidate the ORR mechanism, there still exists controversy on the essentials of the mechanism, and the factors responsible for the slow kinetics of the ORR are uncertain[1].

Car-Parrinello molecular dynamics (CPMD) simulations have been recently carried out in an effort to provide new insights into the ORR mechanism.[2,3] We note that although the reaction mechanism may quantitatively depends on a number of factors, including electrode potential, electrolyte, and adsorbate coverage, the main features of the ORR mechanism may be provided, at least qualitatively, by ab initio molecular dynamics simulations. Using the mechanism obtained with CPMD as a working mechanism, Dynamic Monte Carlo (DMC) simulations are carried out where all reactions are included. The reaction mechanism in this experiment is a ten reaction set, shown in Table 1-1, with activation energies and prefactors for each reaction[1].

The study of a bimetallic surface in contrast to a pure platinum surface also yields considerable interest because the secondary metal can lower the overpotential of the reaction, easily facilitating the slow kinetics of the reaction[4]. Also, costs can come into play with a bimetallic surface, allowing for the catalyst surface to decrease in overall cost by substituting a relatively cheaper metal to achieve the same or even lower overpotentials. In my experiments, though, the metal medium chosen is a non-descript metal, with its only characteristics coming from the different activation energies of the electron transfer reactions and different initial concentrations[4].

Table 1-1: Activation Energies and Prefactors for the Platinum Surface

| | Reaction | Ei (eV) | ν ($s^{-1}$) |
|---|---|---|---|
| I | $O_2 + H^+ + e^- \rightarrow OOH_{ads}$ (b) | 0.45 * | 1.00E2 ** |
| II | $OOH_{ads}$ (b) $\rightarrow$ $O_{ads}$ (t) + $OH_{ads}$ (t) | 0.25 * | 5.1E12 * |
| III | $OH_{ads}$ (t) $\rightarrow$ $OH_{ads}$ (b) | 0.60 * | 1.00E13 ** |
| IV | $OOH_{ads}$ (b) + $H^+ + e^- \rightarrow OHOH_{ads}$ (t) | 0.10 * | 1.00E5 ** |
| V | $OHOH_{ads}$ (t) $\rightarrow$ $OH_{ads}$ (t) + $OH_{ads}$ (t) | 0.30 * | 1.17E11 * |
| VI | $O_{ads}$ (t) + $OH_{ads}$ (t) + $H^+ + e^- \rightarrow H_2O_{ads}$ (t) + $O_{ads}$ (t) | 0.10 * | 1.00E5 ** |
| VII | H2Oads (t) + $O_{ads}$ (t) $\rightarrow$ $OH_{ads}$ (t) + $OH_{ads}$ (t) | 0.10 * | 1.00E13 ** |
| VIII | 2 $OH_{ads}$ (t) + $H^+ + e^- \rightarrow H_2O_{ads}$ (t) + $OH_{ads}$ (t) | 0.60 * | 1.00E8 ** |
| IX | $OH_{ads}$ (t) + $H_2O_{ads}$ (t) + $H^+ + e^- \rightarrow$ 2 $H_2O_{ads}$ (t) | 0.40 * | 1.00E 4 ** |
| X | $H2O_{ads}$ (t) $\rightarrow$ $H_2O$ | 0.60* | 1.00E+13*** |

* values were taken from CPMD and DFT results and

** values were estimated using transition state theory

*** M. Forsth, F. Gudmundson, J.L. Persson, and A. Rosen, A., *Comb. and Flame*, **119**, 144 (1999).

## 2. DMC Methodology and Simulations

The program CARLOS 4.0[1] was employed for the current DMC simulations. The DMC program can be used to simulate all kind of chemical reactions on crystal surfaces.[5,6] The crystal surface is represented by a two-dimensional lattice of unit cells with periodic boundary conditions.

The DMC algorithm implemented in the program CARLOS 4.0[7] is based on the master equation:

$$\frac{dP_\gamma}{dt} = \sum_\beta \left( W_{\gamma\beta} P_\beta - W_{\beta\gamma} P_\gamma \right) \qquad (1)$$

where $P_\gamma$ is the probability to find the system in a given configuration $\gamma$. A configuration is a distribution of particles on a grid, which models the surface and the adsorbed species. $W_{\gamma\beta}$, transition probability per unit time, specifies the rate of the process going from configuration $\gamma$ to configuration $\beta$.

Several methods have been developed for the numerical implementation of the master equation.[7,8] The first-reaction method (FRM)[9] appropriate for cases where reaction constants vary with time, was used in the present study. According to this method, when

the system is in a given configuration $\gamma$, the set of all possible reactions is determined, and a time of occurrence $t_{\gamma\beta}$[9] is generated for each reaction compatible with configuration $\alpha$, according to equation (2), where $W_{\gamma\beta}$ is the time dependent rate of reaction $i$, and $r$ is a random number selected uniformly in the interval (0,1).

$$\exp\left[-\int_{t}^{t_{\gamma\beta}} dt' W_{\gamma\beta}(t')\right] = r \tag{2}$$

Then, the reaction with the smallest $t_{\gamma\beta}$ is selected, the configuration is changed accordingly, and the time $t$ is incremented in $t_{\gamma\beta}$. Finally, the set of possible reactions is generated according to the new configuration $\beta$, and the procedure is repeated. The microscopic rates, $W_{\gamma\beta}$, are related to the individual rate constants $k_i$ by:

$$\begin{aligned} W_{\gamma\beta} &= \sum_i k_i \Delta^i_{\gamma\beta} \\ k_i &= \nu_i \exp\left[-\frac{E_{ai}}{RT}\right] \end{aligned} \tag{3}$$

where the summation runs over all reaction types $i$ with rate constants $k_i$, $\Delta^i_{\gamma\beta} = 1$ when a reaction $i$ can change a configuration $\gamma$ into $\beta$ and zero otherwise, $\nu_i$ is the pre-exponential factor, and $E_{ai}$ is the activation energy of a reaction $i$.

For electrochemical reactions, it is necessary to introduce the potential dependence of the reaction rate. In the presence of an overpotential $\eta$ (defined as the difference between the actual and the equilibrium potential), the microscopic rate of a reaction $i$, $W_i$, is given by the Butler-Volmer potential dependence of the rate constant:[Bard, 2000 #1109]

$$W_i = \nu_i \exp\left(-\frac{E_{ai}(V)}{K_B T}\right) = \nu_i \exp\left(-\frac{\left(E_{ai}(0) + \alpha e_0 \eta\right)}{K_B T}\right) \tag{4}$$

in which the activation energy $E_{ai}$, is potential dependent, modeled in equation (4) as a linear function of the overpotential, $\eta$. $e_0$ is the charge of an electron, and $\alpha$ is the transfer coefficient, which may be a function of the potential.[10]

On the basis of CPMD results, some restrictions were imposed for the working mechanism during DMC simulations. According to our model, the reaction of HO* in

reactions VI, VIII, and IX is always accompanied by a co-adsorbed oxide, such as O* in VI, O*H in VIII and $H_2O$* in IX. Although these co-adsorbed oxides apparently can be removed from these stoichiometric reactions, CPMD simulations indicate that such co-adsorbed oxides do affect the hydrogenation reactions of HO* probably by hydrogen bonding. The effect of co-adsorption on hydrogenation has also been found by Gong et al.[Gong, 2004 #1105] Thus, the adsorbed O*H has a neighbor O*, or OH*, and water has a neighbor $H_2O$*, in reactions VI, VIII, and IX respectively. Our model also includes lateral interactions for the adsorbed HOO*, which allows us to describe the O-O repulsion found in the first step, and also to describe the possible effect on the dynamic surface coverage. Once the OOH is adsorbed, a first neighbor repulsion is imposed, and after the OOH either decomposes or proceeds to the second transfer step, the imposed repulsion is removed. On the other hand no repulsions were imposed between $H_2O$-$H_2O$ and OH-OH adsorbed on the surface and for this reason the OH concentration increases steadily reaching a maximum fractional coverage of 0.79 at about 0.87 V[1].

The crystal surface is represented by a two-dimensional lattice of unit cells containing top, bridge, and hollow adsorption sites, arranged on a (111) plane of 64×64 Pt and M atoms with periodic boundary conditions. The area of the Pt (111) and M (111) unit cell, $6.67 \times 10^{-16}$ $cm^2$, was estimated on the basis of geometric calculations considering a hard-sphere model for the Pt and M atoms. The overpotential, $\eta$, was decreased linearly from 0.0 V until a final value of –0.75 V at a rate of 20 mV/sec, starting with a bimetallic Pt (111) and M (111) surface. The concentration of each of these atoms varied in each trial run, corresponding to 0-90% M and 100-10% Pt atoms. The 100% M (111) case was not studied because no reactions occurred on the surface over the given applied potentials. This range corresponds to applied potentials (V) from 1.23 to 0.48 V (referred to the SHE, standard hydrogen electrode).

The design of the initial input file containing the bimetallic surface was created using a spreadsheet program, with the help of a few macro programs behind it. In order to accurately simulate a random bimetallic surface, a 64 by 64 grid of numbers ranging 0 to 9 needed to be generated and checked for correct concentration of cells, For example, to generate a 20% M (111) surface, a 64 by 64 grid of numbers would need to contain approximately 20% of 1's and 2's to be used. If it did not, a new grid would be generated

until the needed percentage could be achieved. Once the grid of integers was in place, a macro program would check each cell, and the cells to the right of it, to the upper right diagonal and to the top cell neighboring it, to detect if any of those cells contained an integer needed to fulfill the given concentration of M(111) requirement. It needed to check each of those cells because the unit cell's properties depend on those cells around it for its bridging sites. Once it checked each cell and those around it, a final macro program would sweep each cell, assigning a designation for each of the six specified sites, either a t h h b b b for a given Pt(111) atom or a Mt Mh Mh Mb Mb Mb for a given M(111) atom or neighboring atom.

The activation energies shown in Table 1-1 refer to those at zero overpotential, $E_{ai}(0)$. The dependence of the activation energy on the applied potential is taken into account by the relation, $E_{ai}(V) = E_{ai}(0) + \alpha\eta$, shown by equation (4). Only activation energies for the electron-involved reactions are considered to be functions of the overpotential (equation 4).

The activation energies shown in Table 1-2 and 1-3 refer to those at zero overpotential, $E_{ai}(0)$ for the secondary bimetallic M. The activation energies for reactions I, IV, VI, VIII, and IX were modified for two different cases, the first shown in Table 1-2 with reaction I's activation energy doubled and the other reactions activation energy reduced by 10% compared to Pt's activation energy, and the second shown in Table 1-3 with reaction I's activation energy increase by 10% and the other reactions activation energy reduced by 10% compared to Pt's activation energy.

Table 1-2: Activation Energies and Prefactors for the Bimetallic Surface Case I

| | **Reaction** | **Ei (eV)** | **ν ($s^{-1}$)** |
|---|---|---|---|
| **I** | $O_2 + H^+ + e^- \rightarrow OOH_{ads}$ (b) | **0.90 *** | **1.00E2 ***** |
| **II** | $OOH_{ads}$ (b) $\rightarrow$ $O_{ads}$ (t) + $OH_{ads}$ (t) | **0.25 **** | **5.1E12 **** |
| **III** | $OH_{ads}$ (t) $\rightarrow$ $OH_{ads}$ (b) | **0.60 **** | **1.00E13 ***** |
| **IV** | $OOH_{ads}$ (b) + $H^+ + e^-$ $\rightarrow$ $OHOH_{ads}$ (t) | **0.09 *** | **1.00E5 ***** |
| **V** | $OHOH_{ads}$ (t) $\rightarrow$ $OH_{ads}$ (t) + $OH_{ads}$ (t) | **0.30 **** | **1.17E11 **** |
| **VI** | $O_{ads}$ (t) + $OH_{ads}$ (t) + $H^+ + e^-$ $\rightarrow$ $H_2O_{ads}$ (t) + $O_{ads}$ (t) | **0.09 *** | **1.00E5 ***** |
| **VII** | H2Oads (t) + $O_{ads}$ (t) $\rightarrow$ $OH_{ads}$ (t) + $OH_{ads}$ (t) | **0.10 **** | **1.00E13 ***** |
| **VIII** | 2 $OH_{ads}$ (t) + $H^+ + e^-$ $\rightarrow$ $H_2O_{ads}$ (t) + $OH_{ads}$ (t) | **0.54 *** | **1.00E8 ***** |

| | | | |
|---|---|---|---|
| IX | $OH_{ads}$ (t) + $H_2O_{ads}$ (t) + $H^+$ + $e^-$ → 2 $H_2O_{ads}$ (t) | 0.36 * | 1.00E 4 *** |
| X | $H2O_{ads}$ (t) → $H_2O$ | 0.60** | 1.00E+13**** |

* values were modified by 100% and 10% from those given for Pt
** values were taken from CPMD and DFT results and
*** values were estimated using transition state theory
**** M. Forsth, F. Gudmundson, J.L. Persson, and A. Rosen, A., *Comb. and Flame*, **119**, 144 (1999).

Table 1-3: Activation Energies and Prefactors for the Bimetallic Surface Case II

| | Reaction | Ei (eV) | ν ($s^{-1}$) |
|---|---|---|---|
| I | $O_2$ + $H^+$ + $e^-$ → $OOH_{ads}$ (b) | 0.495 * | 1.00E2 *** |
| II | $OOH_{ads}$ (b) → $O_{ads}$ (t) + $OH_{ads}$ (t) | 0.25 ** | 5.1E12 ** |
| III | $OH_{ads}$ (t) → $OH_{ads}$ (b) | 0.60 ** | 1.00E13 *** |
| IV | $OOH_{ads}$ (b) + $H^+$ + $e^-$ → $OHOH_{ads}$ (t) | 0.09 * | 1.00E5 *** |
| V | $OHOH_{ads}$ (t) → $OH_{ads}$ (t) + $OH_{ads}$ (t) | 0.30 ** | 1.17E11 ** |
| VI | $O_{ads}$ (t) + $OH_{ads}$ (t) + $H^+$ + $e^-$ → $H_2O_{ads}$ (t) + $O_{ads}$ (t) | 0.09 * | 1.00E5 *** |
| VII | $H2O_{ads}$ (t) + $O_{ads}$ (t) → $OH_{ads}$ (t) + $OH_{ads}$ (t) | 0.10 ** | 1.00E13 *** |
| VIII | 2 $OH_{ads}$ (t) + $H^+$ + $e^-$ → $H_2O_{ads}$ (t) + $OH_{ads}$ (t) | 0.54 * | 1.00E8 *** |
| IX | $OH_{ads}$ (t) + $H_2O_{ads}$ (t) + $H^+$ + $e^-$ → 2 $H_2O_{ads}$ (t) | 0.36 * | 1.00E 4 *** |
| X | $H2O_{ads}$ (t) → $H_2O$ | 0.60** | 1.00E+13**** |

* values were modified by 10% from those given for Pt
** values were taken from CPMD and DFT results and
*** values were estimated using transition state theory
**** M. Forsth, F. Gudmundson, J.L. Persson, and A. Rosen, A., *Comb. and Flame*, **119**, 144 (1999).

## 3. Results and Discussions

The following are analyses of the two cases stated above, found in Tables 1-2 and 1-3, for different initial concentrations of M (111).

*Case I*

The data presented in the following tables and graphs were taken at a current density of -1 mA/$cm^2$ and had an activation energy, Ea, for adsorption of oxygen onto the secondary metal of 2*Ea of platinum.

Table 2-1: Total top sites Occupied at current density of -1

| Potential | M Conc. | M top sites used | Pt top sites used | Total Top sites used |
|---|---|---|---|---|
| 0.810 | 0.50 | 3.72% | 6.74% | 10.46% |
| 0.810 | 0.70 | 2.97% | 5.27% | 8.24% |
| 0.810 | 0.60 | 3.03% | 5.20% | 8.23% |
| 0.806 | 0.40 | 3.75% | 8.45% | 12.20% |
| 0.802 | 0.30 | 3.90% | 8.90% | 12.80% |
| 0.798 | 0.80 | 2.35% | 5.75% | 8.10% |
| 0.790 | 0.00 | 0.00% | 18.65% | 18.65% |
| 0.788 | 0.10 | 1.61% | 16.34% | 17.95% |
| 0.788 | 0.20 | 3.70% | 12.54% | 16.24% |
| 0.780 | 0.90 | 1.29% | 8.94% | 10.23% |

Table 2-2: Total OH absorbed at current density of -1

| Potential | M Conc. | OH t Conc. | OHMt Conc. | Total OH Conc. |
|---|---|---|---|---|
| 0.810 | 0.50 | 6.59% | 3.47% | 10.06% |
| 0.810 | 0.70 | 5.29% | 2.55% | 7.84% |
| 0.810 | 0.60 | 5.31% | 2.69% | 8.00% |
| 0.806 | 0.40 | 8.02% | 3.48% | 11.50% |
| 0.802 | 0.30 | 8.48% | 3.50% | 11.98% |
| 0.798 | 0.80 | 5.86% | 1.92% | 7.78% |
| 0.790 | 0.00 | 16.53% | 0.00% | 16.53% |
| 0.788 | 0.10 | 15.19% | 1.47% | 16.65% |
| 0.788 | 0.20 | 11.99% | 2.56% | 14.56% |
| 0.780 | 0.90 | 8.06% | 1.19% | 9.25% |

Table 2-3: Total O absorbed at current density of -1

| Potential | M Conc. | Ot Conc. | OMt Conc. | Total Ot Conc. |
|---|---|---|---|---|
| 0.810 | 0.50 | 0.20% | 0.20% | 0.39% |
| 0.810 | 0.70 | 0.00% | 0.42% | 0.42% |
| 0.810 | 0.60 | 0.12% | 0.20% | 0.33% |
| 0.806 | 0.40 | 0.37% | 0.37% | 0.73% |
| 0.802 | 0.30 | 0.42% | 0.33% | 0.74% |
| 0.798 | 0.80 | 0.00% | 0.37% | 0.37% |
| 0.790 | 0.00 | 2.05% | 0.00% | 2.05% |
| 0.788 | 0.10 | 1.09% | 0.00% | 1.09% |
| 0.788 | 0.20 | 0.73% | 0.37% | 1.10% |
| 0.780 | 0.90 | 0.00% | 0.19% | 0.19% |

From this case, it was determined to separate the initial M concentrations into 3 groups and discuss each group accordingly.

The first group of initial M concentrations is the 50, 70 and 60 percent initial M concentration. These performed the best, showing a 0.02 improvement over the control Platinum surface. These results can be attributed to the optimum availability of sites available, showing that the top site for both metals is being used. The 50% performs the best, as shown in the graph below, but also in the fact that it has the greatest percent of occupied top sites in the group (Table 2-1), allowing for more reactions to occur (especially reaction 8, as shown on Graph 2-2). Also, at 50% M concentration, OH is maximized in the group, the key molecule in reaction 8. The correlation of OH concentration being maximized on the M surface and minimized on the Pt surface is realized on Graph 2-3 below.

The second group of initial M concentrations is the 40, 30 and 80 percent initial M concentration. These also performed better than the control; though not as much as the first group. This can be attributed to the fact that these initial concentrations performed very similarly to the control experiment, though with the addition of the M metal, it facilitated the electroreduction more readily. This can be seen in the above tables for that they perform somewhat close to the control, but enhance the control due to the availability of the metal M.

The third group of initial M concentrations is the 10, 20 and 90 percent initial M concentrations. These concentrations actually hindered electroreduction instead of facilitating in comparison to the control. For the 10 and 20 percent, an explanation for this is the fact that surface is almost pure Platinum, with the metal M acting as a non-reactant instead of as a facilitator. The metal M has comparative high activation energy for the initial reaction, the absorption of oxygen, and since the concentration of M is low

in comparison to the concentration of Pt, it hinders the overall current density. The same holds true for the 90% M concentration, only in reverse. Since the metal M cannot absorb the oxygen needed, the 10% Pt bottlenecks the overall reaction.

Graph 2-1: Current Density for Case I

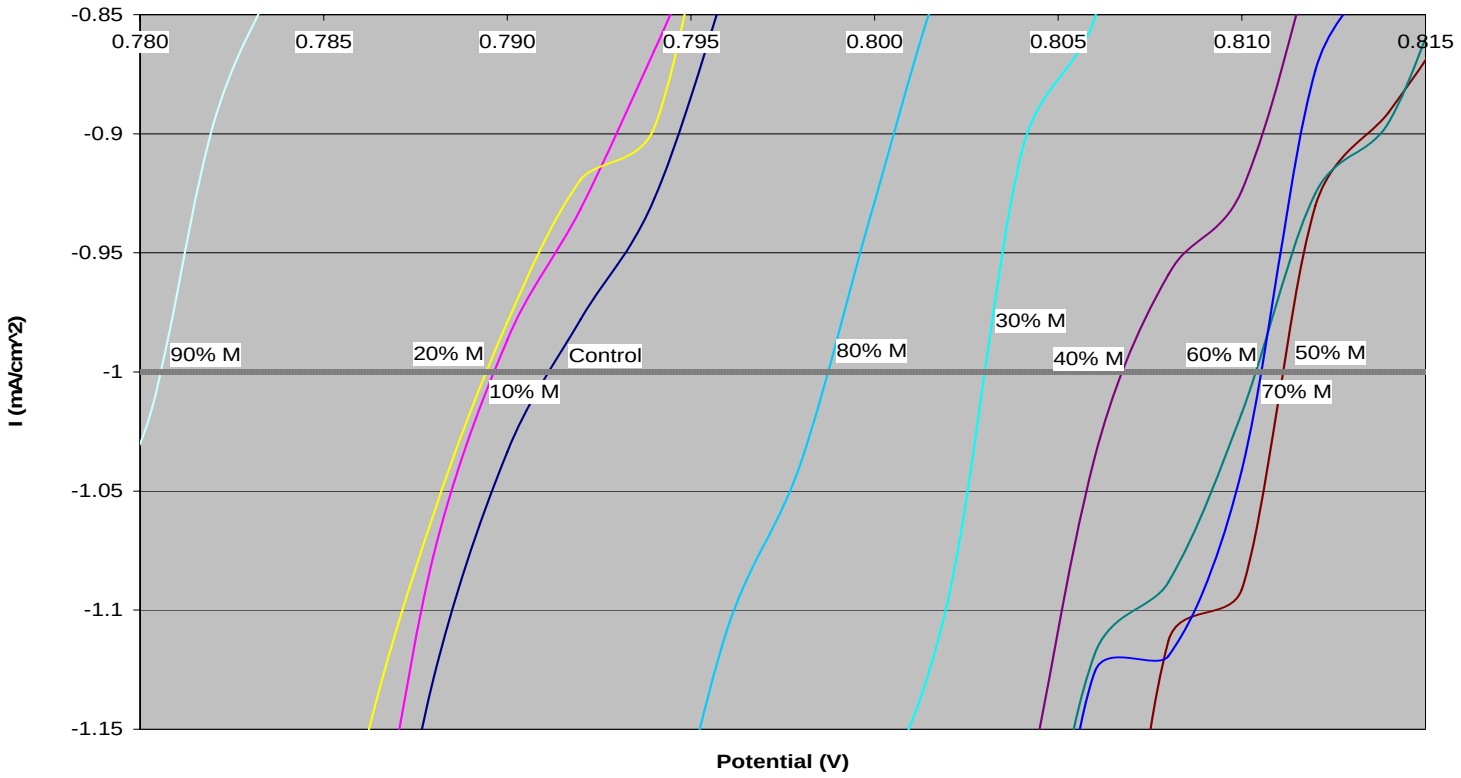

Graph 2-2: Reaction 8 Rates for Case I

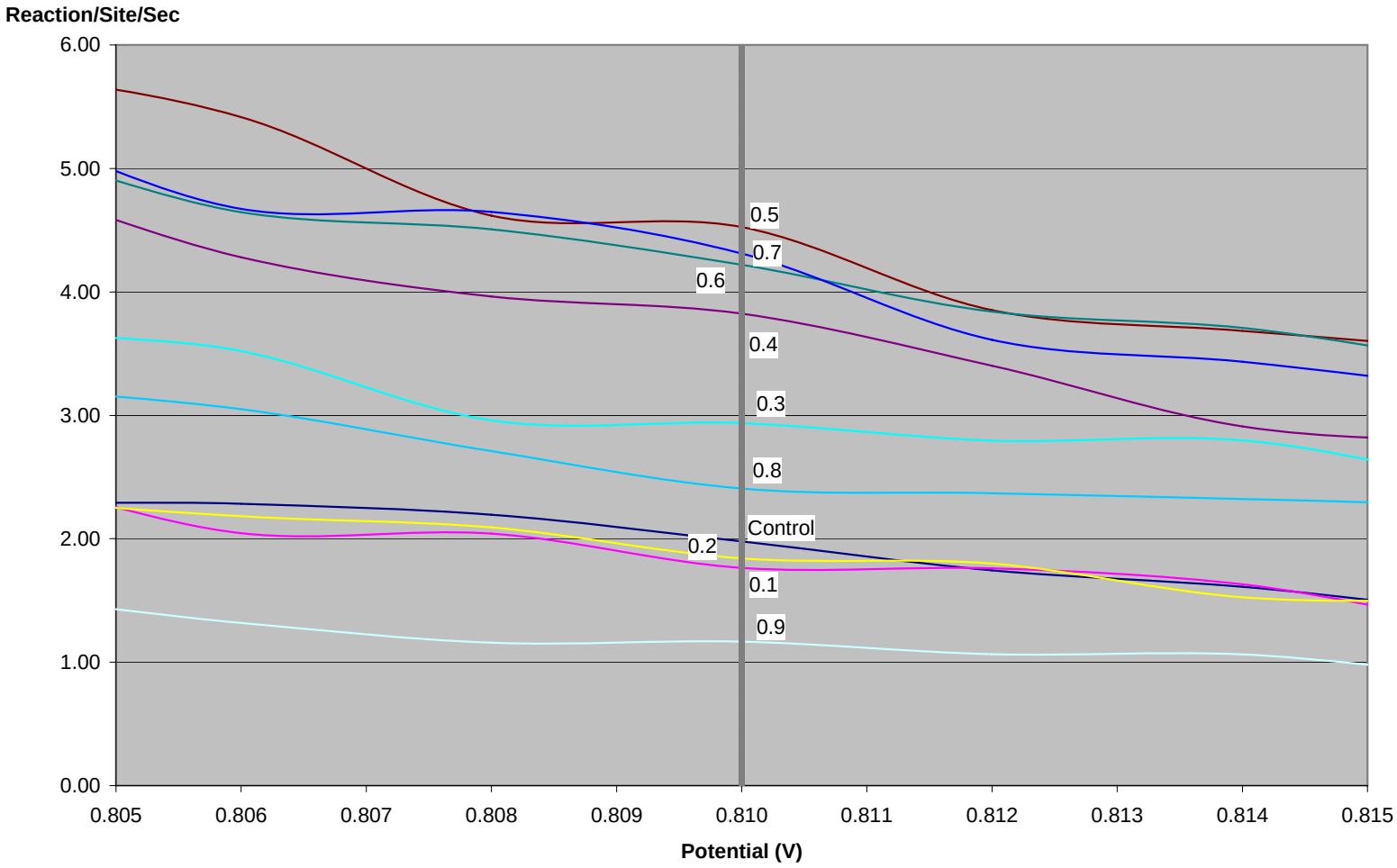


The overall controlling reaction for this electroreduction is reaction 8, the same reaction found to be primarily controlling the Platinum only surface case. As seen above, the Reaction/Site/Sec almost mirrors the results of the current density for each metal M initial concentration, with the exception of the 10 and 20 percent M concentration. This is just a scale error, for I have shown the reaction 8 rates at a potential of 0.810, the potential where the first concentrations start to show, though for 10 and 20 percent M, their potential does not reach -1 mA/cm2 until 0.788.

Graph 2-3: OH absorbed at -1 mA/cm$^2$ for Case I

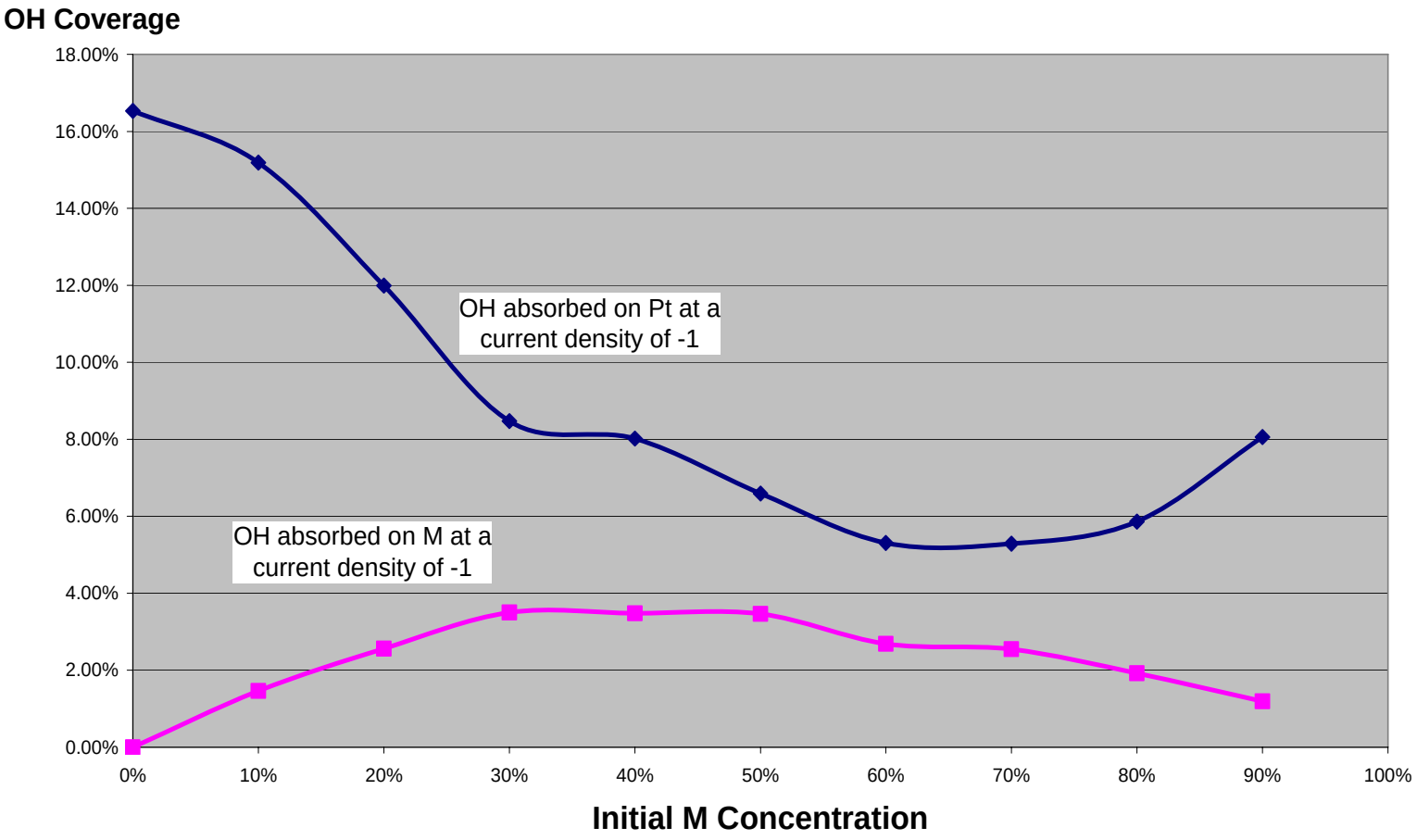


From Graph 2-3, in the range of initial M concentrations show to work the best, 50%-70 percent, the coverage of OH on Pt is minimized while the coverage of OH on M is maximized. This suggests that in order for the ORR to be facilitated on a bimetallic surface, the OH concentration needs to be maximized on the secondary metal and minimized on Pt.

The overpotential, the needed voltage to sustain a continuous current density, for each of the initial M concentrations is shown in Table 2-4.

Table 2-4: Overpotential taken at first continuous current density potential for Case I

| M Conc. | Overpotential (V) |
|---|---|
| 40% | 0.218 |
| 30% | 0.240 |
| 50% | 0.248 |
| 80% | 0.258 |
| 70% | 0.264 |
| 10% | 0.268 |
| 60% | 0.270 |
| 20% | 0.276 |
| 90% | 0.280 |
| 0% | 0.280 |

The overpotential does not follow the above stated results taken at -1 mA/cm$^2$, which is understandable for the fact that it is measured at the potential where a continuous current density is shown, while the data above is shown at a current density of -1 mA/cm$^2$. This can be seen that for a given concentration, the current density can initially flow at a higher voltage, but level out at a lower level, allowing other concentrations to perform better. Although it does not follow the above stated results in concentration performance groupings, it does demonstrate that all the initial M concentrations perform better that the Pt only surface initially, though the pattern quickly returns to the data shown for -1 mA/cm$^2$.

*Case II*

The data presented in the following tables and graphs were taken at a current density of -1 mA/cm$^2$ and had an activation energy, Ea, for adsorption of oxygen onto the secondary metal of 1.1*Ea of platinum.

Table 3-1: Total top sites Occupied at current density of -1

| Potential | M Conc, | M top sites used | Pt top sites used | Total Top sites used |
|---|---|---|---|---|
| 0.820 | 60% | 4.05% | 5.95% | 10.00% |
| 0.818 | 50% | 4.30% | 6.34% | 10.64% |
| 0.816 | 70% | 3.84% | 5.93% | 9.78% |
| 0.816 | 80% | 4.18% | 4.40% | 8.57% |
| 0.812 | 90% | 3.72% | 6.74% | 10.46% |
| 0.806 | 40% | 4.00% | 7.60% | 11.60% |
| 0.798 | 30% | 3.90% | 8.56% | 12.46% |
| 0.796 | 20% | 3.45% | 10.95% | 14.40% |
| 0.790 | 0% | 0.00% | 18.65% | 18.65% |
| 0.788 | 10% | 4.30% | 14.60% | 18.90% |

Table 3-2: Total OH absorbed at current density of -1

| Potential | M Conc, | OH t Conc. | OHMt Conc. | Total OHt Conc. |
|---|---|---|---|---|
| 0.820 | 60% | 5.98% | 3.54% | 9.52% |
| 0.818 | 50% | 6.30% | 3.96% | 10.25% |
| 0.816 | 70% | 5.86% | 3.42% | 9.28% |
| 0.816 | 80% | 4.52% | 3.57% | 8.09% |
| 0.812 | 90% | 5.86% | 3.31% | 9.17% |
| 0.806 | 40% | 7.20% | 3.91% | 11.11% |
| 0.798 | 30% | 8.30% | 3.50% | 11.80% |
| 0.796 | 20% | 10.59% | 2.69% | 13.28% |
| 0.790 | 0% | 16.53% | 0.00% | 16.53% |
| 0.788 | 10% | 13.46% | 3.91% | 17.36% |

Table 3-3: Total O absorbed at current density of -1

| Potential | M Conc, | Ot Conc. | OMt Conc. | Total Ot Conc. |
|---|---|---|---|---|
| 0.820 | 60% | 0.12% | 0.37% | 0.49% |
| 0.818 | 50% | 0.10% | 0.29% | 0.39% |
| 0.816 | 70% | 0.08% | 0.42% | 0.50% |
| 0.816 | 80% | 0.00% | 0.55% | 0.55% |
| 0.812 | 90% | 0.00% | 0.52% | 0.52% |
| 0.806 | 40% | 0.33% | 0.18% | 0.51% |
| 0.798 | 30% | 0.28% | 0.33% | 0.60% |
| 0.796 | 20% | 0.55% | 0.00% | 0.55% |
| 0.790 | 0% | 2.05% | 0.00% | 2.05% |
| 0.788 | 10% | 1.17% | 0.24% | 1.41% |

From this case, it was determined to separate the initial M concentrations into 2 groups and discuss each group accordingly.

The first group is composed of the initial M concentrations of 50-90%. These concentrations performed the best in comparison to the control Pt surface, with 60% initial M concentration performing the best. These results differ from those in Case I by the simple fact that in this case, the adsorption of oxygen can take place onto the secondary metal whereas it could not before. Because of this, the higher the initial concentration of M, the lower the voltage needed to create current density. Unlike before, where the 80% and 90% did not perform as great as the other higher concentrations, it does perform closer to the other higher concentrations here, validating the results that in Case I, the secondary metal acts as a hindrance instead of a facilitator.

The second group is composed of the initial M concentrations of 10-40%. These concentrations, with the exception of 10%, also performed better than the control surface, though not as well as the first group. This group though does demonstrate the trend stated for the first group in that the higher the concentration of M, the lower the voltage needed to generate current density. This is seen in that 40% is followed by 30% is followed by 20% in their performance in this group. Only the initial M concentration of 10% still performs worst than the control Pt surface, for which this can be attributed to the fact that it still acts as a hindrance, and without more sites of the reduced activation energy, it cannot perform as well. These current densities can be seen in the following graph 3-1.

Graph 3-1: Current Density for Case II

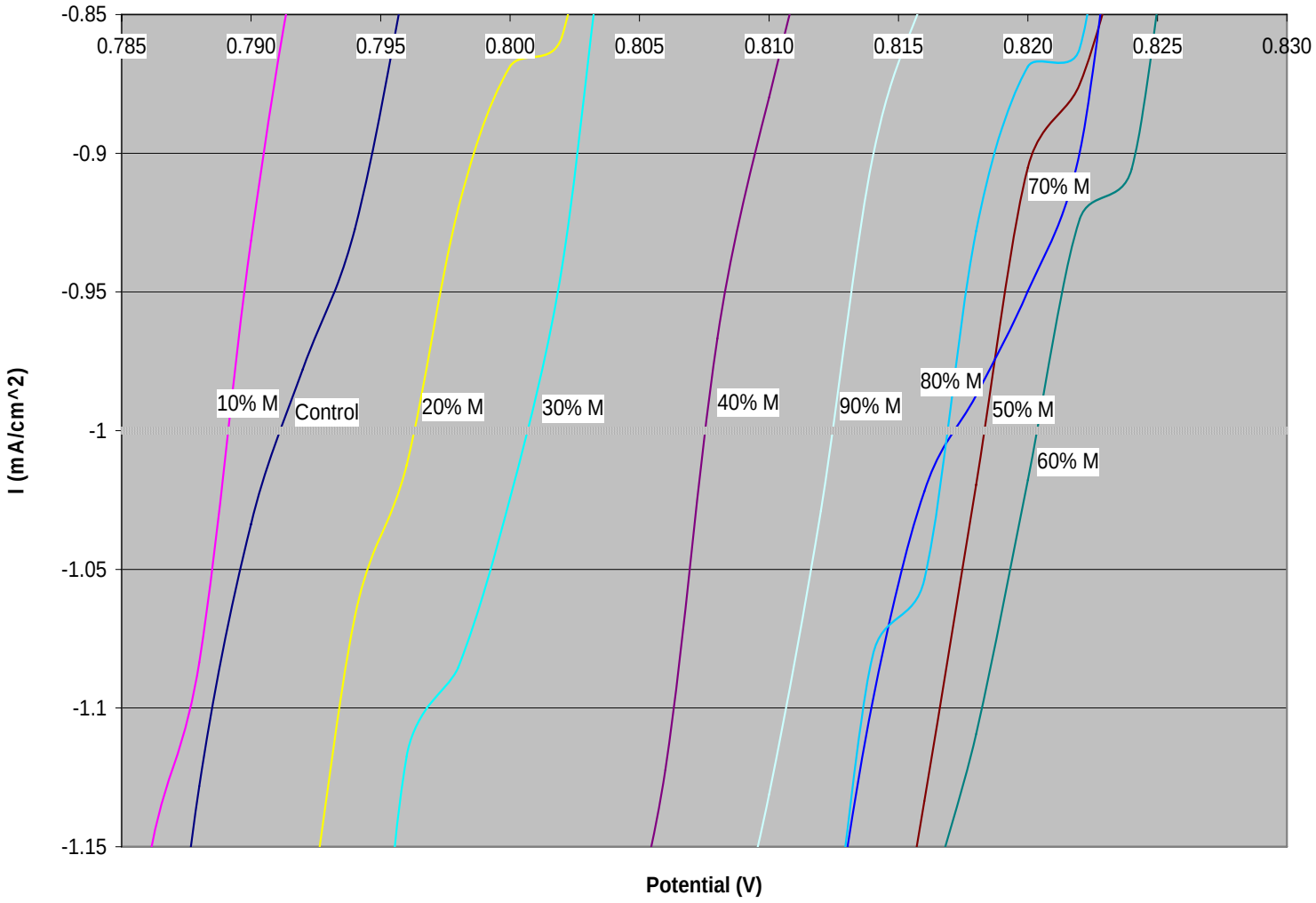

Graph 3-2: OH absorbed at -1 mA/cm$^2$ for Case II

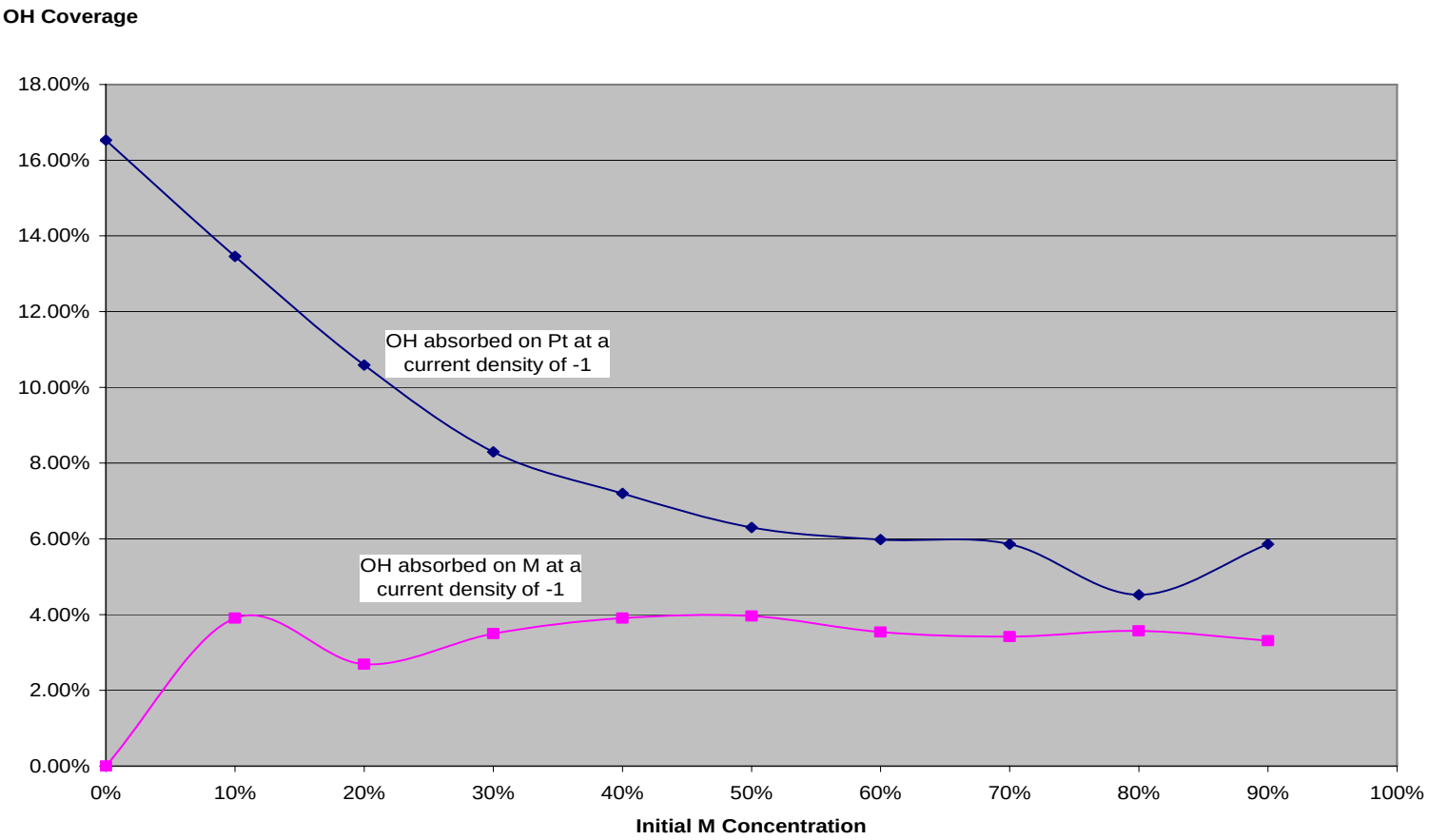


From Graph 3-2, in the range of initial M concentrations show to work the best, 50%-90%, the coverage of OH on Pt is minimized while the coverage of OH on M is maximized, just like before in Case 1. Case II illustrates that the same results gathered from Case I holds true to Case II, with the exception of 80%, for the concentration of OH on Pt is lower than that of the surrounding concentrations. This can be inferred as an anomalous data point.

The overpotential, the needed voltage to sustain a continuous current density, for each of the initial M concentrations in Case II is shown in Table 3-4.

Table 3-4:Overpotential taken at first continuous current density potential for Case II

| M Conc. | Overpotential (V) |
|---|---|
| 30% | 0.220 |
| 70% | 0.228 |
| 80% | 0.242 |
| 40% | 0.246 |
| 20% | 0.248 |
| 60% | 0.254 |
| 50% | 0.264 |
| 90% | 0.270 |
| 0% | 0.280 |
| 10% | 0.286 |

Similarly, the overpotential for Case II also does not follow the above stated results taken at -1 mA/cm$^2$, which is understandable for the fact that it is measured at the potential where a continuous current density is shown, while the data above is shown at a current density of -1 mA/cm$^2$. The same conclusions can be drawn about these overpotentials as were seen from Case I.

## 4. Conclusions

It has been shown that utilizing a bimetallic surface with lower activation energy does lower the potential needed to sustain a current density for the ORR. In looking at the first case, which has a 10% reduction in the activation energy in the four electron reactions of ORR and a 100% increase in the activation energy of oxygen absorbing onto M, that 50% M concentration yields the greatest current density and 40% M concentration yields the best overpotential. In looking at the second case, which has a 10% reduction in the activation energy in the four electron reactions of ORR and a 10% increase in the activation energy of oxygen absorbing onto M, that 60% M concentration yields the greatest current density and 30% M concentration yields the best overpotential.

**References:**


1. Calvo, S.R., et al., *Dynamic Monte Carlo simulations of the oxygen electroreduction reaction on a Pt(111) surface.* J. Phys. Chem. B, 2005: p. to be submitted.
2. Wang, Y. and P.B. Balbuena, *Ab initio-molecular dynamics studies of $O_2$ electroreduction on Pt (111): Effects of proton and electric field.* J. Phys. Chem. B, 2004. **108**: p. 4376-4384.
3. Wang, Y. and P.B. Balbuena, *Ab initio Molecular Dynamics Simulations of the Oxygen Electroreduction Reaction on a Pt(111) Surface in the Presence of Hydrated Hydronium $(H_3O)+(H_2O)_2$: Direct or Series Pathway?* J. Phys. Chem. B, 2005. **109**: p. 14896-14907.
4. Wang, Y. and P.B. Balbuena, *Design of oxygen reduction bimetallic catalysts: Ab-initio derived thermodynamic guidelines.* J. Phys. Chem. B, 2005. **109**(40): p. 18902-18906.
5. Mainardi, D.S., et al., *Dynamic Monte Carlo Simulations of $O_2$ Adsorption and Reaction on Pt(111).* Chem. Phys. Lett., 2003. **382**: p. 553-560.
6. Calvo, S.R., et al., *Test of a mechanism for $O_2$ electroreduction on Pt(111) via Dynamic Monte Carlo simulations*, in *Power Sources Modeling*, R.G. Jungst, et al., Editors. 2004, Pennington: NJ.
7. Lukkien, J., et al., *Efficient Monte Carlo methods for the simulation of catalytic surface reactions.* Phys. Rev. E, 1998. **58**(2): p. 2598-2610.
8. Jansen, A.P.J. and J.J. Lukkien, *Dynamic Monte-Carlo simulations of reactions in heterogeneous catalysis.* Catalysis Today, 1999. **53**: p. 259-271.
9. Gelten, R.J., R.A. VanSanten, and A.P.J. Jansen, *Dynamic Monte Carlo simulations of oscillatory chemical reactions*, in *Molecular dynamics: From classical to quantum methods*, P.B. Balbuena and J.M. Seminario, Editors. 1999, Elsevier Science: Amsterdam. p. 737-784.
10. Sidik, R.A. and A.B. Anderson, *Density functional theory study of $O_2$ electroduction when bonded to a Pt dual site.* J. Electroanal. Chem., 2002. **528**: p. 69-76.

# CONTACT INFORMATION


| | |
|---|---|
| Name: | Adam Wayne Wood |
| Address: | PO Box 15435, College Station, TX, 77841-5435 |
| Email Address: | aww0192@neo.tamu.edu |
| Education: | B.S., Chemical Engineering, Texas A&M University-College Station, 2006. |